BJP BRITISH JOURNAL OF PHARMACOLOGY

BPS BRITISH PHARMACOLOGICAL SOCIETY

British Journal of Pharmacology (2010), 159, 1672–1680

0007-1188/10
www.brjpharmacol.org

RESEARCH PAPER

Inhibition of angiotensin-converting enzyme stimulates fracture healing and periosteal callus formation – role of a local renin-angiotensin system

P Garcia[1,2], S Schwenzer[1,2], JE Slotta[2,3], C Scheuer[2,3], AE Tami[4], JH Holstein[1,2], T Histing[1,2], M Burkhardt[1], T Pohlemann[1,2] and MD Menger[2,3]

[1]*Department of Trauma-, Hand- and Reconstructive Surgery, University of Saarland, Homburg/Saar, Germany,* [2]*Collaborative Research Center, AO Foundation,* [3]*Institute for Clinical & Experimental Surgery, University of Saarland, Homburg/Saar, Germany, and* [4]*AO Research Institute, Davos, Switzerland*

Background and purpose: The renin-angiotensin system (RAS) regulates blood pressure and electrolyte homeostasis. In addition, 'local' tissue-specific RAS have been identified, regulating regeneration, cell growth, apoptosis, inflammation and angiogenesis. Although components of the RAS are expressed in osteoblasts and osteoclasts, a local RAS in bone has not yet been described and there is no information on whether the RAS is involved in fracture healing. Therefore, we studied the expression and function of the key RAS component, angiotensin-converting enzyme (ACE), during fracture healing.
Experimental approach: In a murine femur fracture model, animals were treated with the ACE inhibitor perindopril or vehicle only. Fracture healing was analysed after 2, 5 and 10 weeks using X-ray, micro-CT, histomorphometry, immunohistochemistry, Western blotting and biomechanical testing.
Key results: ACE was expressed in osteoblasts and hypertrophic chondrocytes in the periosteal callus during fracture healing, accompanied by expression of the angiotensin type-1 and type-2 receptors. Perindopril treatment reduced blood pressure and bone mineral density in unfractured femora. However, it improved periosteal callus formation, bone bridging of the fracture gap and torsional stiffness. ACE inhibition did not affect cell proliferation, but reduced apoptotic cell death. After 10 week treatment, a smaller callus diameter and bone volume after perindopril treatment indicated an advanced stage of bone remodelling.
Conclusions: Our study provides evidence for a local RAS in bone that influenced the process of fracture healing. We show for the first time that inhibition of ACE is capable of accelerating bone healing and remodelling.
British Journal of Pharmacology (2010) **159,** 1672–1680; doi:10.1111/j.1476-5381.2010.00651.x; published online 5 March 2010

Keywords: rodent; bone; modelling and remodelling; bone histomorphometry; novel entities

Introduction

The renin-angiotensin system (RAS) is classically known as a circulating endocrine system regulating blood pressure and electrolyte homeostasis (Paul *et al.*, 2006). The main effector peptide in this system is angiotensin II (Ang II), which is formed from angiotensin I (Ang I) by angiotensin-converting enzyme (ACE), a key molecule in this system. This precursor, Ang I, is cleaved from angiotensinogen by renin. The effector molecule Ang II exerts its biological effects through binding to different specific angiotensin receptors, mainly the angiotensin types 1 and 2 (AT_1 and AT_2 receptors; nomenclature follows Alexander *et al.*, 2009). ACE furthermore interferes with the kallikrein-kinin system by degradation of bradykinin, which is responsible for prostaglandin (PG) and nitric oxide (NO) production through binding with its specific receptors (B_1 and B_2 receptors).

Besides this classical, systemic RAS, 'local' tissue-specific RASs have been identified in various organs, including heart, kidney, bone marrow, blood vessels and fat tissue (Paul *et al.*, 2006). Independent from the systemic actions of the RAS, the local RAS have been recognized to play an important role in mediating inflammation, angiogenesis, cell proliferation and apoptotic cell death (Haulica *et al.*, 2005).

Little is known, however, about a local RAS in bone (Nakagami *et al.*, 2007; Sernia *et al.*, 2008). Different components of the RAS have been found to be synthesized and to be active in osteoblasts and in osteoclasts (Hatton *et al.*, 1997; Hiruma *et al.*, 1997; Izu *et al.*, 2009). Hatton *et al.* (1997) showed that Ang II stimulated bone resorption in osteoblast and osteoclast co-cultures. The same effect was observed after stimulation

Correspondence: Dr Patric Garcia, Department of Trauma, Hand and Reconstructive Surgery, University of Saarland, D-66421 Homburg/Saar, Germany. E-mail: chpgar@uniklinikum-saarland.de
Received 30 July 2009; revised 16 November 2009; accepted 6 December 2009

with Ang I and was blunted by the ACE inhibitor moexiprilat. This indicates that Ang II is generated by osteoblasts or osteoclasts through conversion of Ang I by ACE. Accordingly, Hatton *et al.* (1997) hypothesized the existence of a local RAS in bone that might play a role in the regulation of bone metabolism. Schurman *et al.* (2004) showed decreased calcium uptake into bone discs after stimulation with Ang II. In addition, Ang II suppresses osteoblastic cell differentiation and bone formation *in vitro*. This effect was caused by specific binding of Ang II to the AT_1 receptor (Hagiwara *et al.*, 1998). Finally, recent studies have now also demonstrated expression of RAS components in osteoblasts and osteoclasts *in vivo* (Izu *et al.*, 2009).

Further evidence for a potential role of the RAS in bone metabolism comes from clinical studies. Patients treated with an ACE inhibitor showed an increased bone mineral density (BMD) and a reduced fracture risk (Perez-castrillon *et al.*, 2003b; Rejnmark *et al.*, 2006; Nakagami *et al.*, 2007). In addition, different studies have shown that a genetic insertion-/deletion polymorphism of ACE (I/D), which determines ACE activity, is associated with inter-individual differences in BMD. These studies have indicated that individuals with the I/I genotype (decreased ACE activity) have a higher BMD than individuals with an I/D or D/D genotype (increased ACE activity) (Woods *et al.*, 2001; Perez-castrillon *et al.*, 2003a). However, there is still little known about the role of the RAS in bone and, particularly about its involvement in the process of fracture healing. We have therefore analysed the expression of ACE and the AT_1 and AT_2 receptors during fracture healing and concluded that inhibition of ACE stimulates fracture healing.

Methods

Animals

All animal care and experimental procedures were performed in adherence to the National Institute of Health guidelines for the use of experimental animals and were approved by the German legislation on the protection of animals (permission code K110/180-07).

Forty eight CD-1 mice of either sex (34 ± 0.3 g; from our own animal facility) were treated daily with the ACE inhibitor perindopril (Coversum® Servier, Munich, Germany) (3 $mg \cdot kg^{-1}$) in their drinking water. An additional 48 mice served as controls, given only drinking water. Animals were killed after 2, 5 and 10 weeks by cervical dislocation. Fracture healing was evaluated by biomechanical (n = 48) and by histomorphometric and immunohistochemical (n = 48) analysis. In some of the animals (n = 7 each group) mean arterial blood pressure (MAP) was analysed after 2, 5 and 10 weeks by cannulation of the right carotid artery (Servomed, Hellige GmbH, Freiburg, Germany). Additional animals were killed after 2 weeks for Western blot analysis (n = 4 each group) and after 10 weeks for micro-CT analysis (n = 7 each group).

Surgical procedure

Mice were anaesthetized by an intraperitoneal injection of 25 $mg \cdot kg^{-1}$ xylazine (Rompun®, Bayer HealthCare, Leverkusen, Germany) and 75 $mg \cdot kg^{-1}$ ketamine (Ketanest®, Pfizer, New York, NY, USA). Under sterile conditions a 4 mm medial parapatellar incision was performed at the right knee, and the patella was dislocated laterally. After drilling a hole (M = 0.5 mm) into the intracondylar notch a distally flattened 24 G needle (Holstein *et al.*, 2007) was implanted intramedullary and the wound was closed. Then the middle of the femur was exhibited through a lateral approach and a custom made clip of 4 mm length was implanted ventro-dorsally in the femur as described previously (Garcia *et al.*, 2008a,b). An osteotomy with a gap size of 0.25 mm was created with a Gigli wire saw. Wound closure completed the operative procedure. For post-operative analgesia, all animals were treated with Carprofen (Rimadyl®, Pfizer) (5 $mg \cdot kg^{-1}$) by daily subcutaneous administration for 3 days. Animals were maintained at the animal care facility at the Institute for Clinical and Experimental surgery, University of Saarland, Germany. A specialized animal technician cared for the animals and checked them daily. Additionally, animals were monitored daily by one of the authors (PG).

Radiological analysis

At the end of the 2, 5 and 10 weeks post fracture observation period, mice were anaesthetized (25 $mg \cdot kg^{-1}$ xylazine and 75 $mg \cdot kg^{-1}$ ketamine), and ventro-dorsal X-rays of the healed femora were taken. Fracture healing was analysed by two observers, without knowledge of the treatments, according to the classification of Goldberg *et al.* (Goldberg *et al.*, 1985) with stage 0 indicating radiological non-union, stage 1 indicating possible union and stage 2 indicating radiological union. Callus diameter was measured in relation to the femur diameter (%) (ImageJ Analysis System, NIH, Bethesda, MD, USA).

Biomechanical analysis

For biomechanical analysis the right and the left femora were resected, carefully freed from soft tissue, the intramedullary pin was removed and the clip was cut in the middle. The proximal and distal ends of the femur were fixed in metallic tubes using polymethylmethacrylate (PMMA), with a working gauge length of 5 mm. The bones were then mounted on a computational based torsional testing device (teststand FMT-400 and digital force gauge FMI-210B2, Alluris, Freiburg, Germany). Applying a gradually increasing angle (0.15 s^{-1}), peak torque at failure (Nmm) and peak rotation angle at failure (°) were measured, and torsional stiffness (Nmm/°) was calculated. To account for differences in bone strength of the individual animals, the non-osteotomized left femora were also analysed, serving as an internal control. Therefore, all values of the osteotomized femora are given in percent of the corresponding values from non-osteotomized femora.

Histomorphometric analysis

After resection, the healed femora were fixed in IHC Zinc fixative (BD Pharmingen, San Diego, CA, USA) for 12–24 h, decalcified in 10% EDTA solution for 3 weeks and embedded in paraffin. The implants were removed after the

decalcification process to preserve fracture morphology. Longitudinal sections of 5 μm thickness were cut and stained according to the trichrome method of Masson and Goldner. At a magnification of 1.25× (Olympus BX60 Microscope, Olympus, Tokyo, Japan; Zeiss Axio Cam and Axio Vision 3.1, Carl Zeiss, Oberkochen, Germany; ImageJ Analysis System, NIH, Bethesda, MD, USA) structural indices were calculated according to the nomenclature and units of the recommendations of the American Society of Bone and Mineral Research (ASBMR): (i) periosteal callus area [Pc.Ar (mm^2)]; (ii) maximum callus diameter/femur diameter (Cl.Dm/F.Dm); (iii) gap width (mm); and (iv) tissue distribution of bone, cartilage and fibrous tissue in the callus area (%). Periosteal callus area was defined by the outer diameter of the callus in the radial direction and 2 mm proximally and distally from the fracture gap in the axial direction. Additionally, we used a score system to evaluate the quality of fracture bridging as described previously (Garcia *et al.*, 2008a,b). Both cortices were analysed for bone bridging (2 points), cartilage bridging (1 point) or bridging with fibrous tissue (0 point). This score system results in a maximum of four points for each specimen, indicating complete bone bridging.

Immunohistochemical analysis

Tissue sections were deparaffinized in xylene and rehydrated in a descending, graded series of alcohol. Endogenous peroxidase was blocked by 3% H_2O_2 (10 min). After blocking nonspecific binding with phosphate-buffered saline and goat normal serum (30 min; room temperature), sections were incubated overnight with a goat anti-mouse ACE monoclonal antibody (1:50 phosphate-buffered saline; Santa Cruz Biotechnology, Santa Cruz, CA, USA) at room temperature. Peroxidase-conjugated rabbit anti-goat (1:100; Dianova, Hamburg, Germany) was used as secondary antibody (incubation for 1 h at room temperature). Diaminobenzidine (DAB; Dako, Glostrup, Denmark) served as the chromogen and Mayer's hemalum as the counterstain.

Western blot

The callus tissue was frozen and stored at –80°C until required. Specimens were homogenized and extracted in lysis buffer consisting of 10 mM Tris pH 7.5, 10 mM NaCl, 0.1 mM EDTA, 0.5% Triton-X 100, 0.02% NaN_3, 0.2 mM PMSF and protease inhibitor cocktail (1:100; Sigma, Taufkirchen, Germany). Proteins were separated and transferred to membranes by standard protocols and probed using anti-proliferating cell nuclear antigen (PCNA; 1:250; Dako Cytomation, Hamburg, Germany), anti-caspase-3 (1:200; Cell Signaling Technology; Frankfurt, Germany), anti-AT_1 receptor (1:100; Santa Cruz Biotechnology) and anti-ACE antibodies (1:500; Santa Cruz Biotechnology). Protein expression was visualized by means of luminol enhanced chemiluminescence (ECL, Amersham Biosciences, Freiburg, Germany) after exposure of the membrane to a blue-light-sensitive autoradiography film (Hyperfilm ECL, Amersham Biosciences). Signals were densitometrically assessed (Geldoc, Quantity one software; Bio-Rad, Hercules, CA, USA) and normalized to the β-actin signals (mouse monoclonal anti-β-actin antibody, 1:20 000; Sigma, St. Louis, USA) to correct for unequal loading.

Micro-CT analysis

Right and left femora were measured with a microtomographic imaging system (μCT 40, Scanco Medical, Brüttisellen, Switzerland) and analysed by a single operator. Two-dimensional CT images were reconstructed in 1024-1024 pixel matrices from 500 projections using a standard convolution-backprojection procedure. Images were stored in 3-D arrays with an isotropic voxel size of 12 μm. Volume of interest (VOI) in right fractured femora was defined by the entry points of the metallic clip (proximal and distal of the osteotomy) in the axial direction and by the outer diameter of the callus in the radial direction. This resulted in a 2.5 mm thick square cuboid comprising any mineralized tissue surrounding the fracture. A 3-D Gaussian filter with a sigma of 0.8 and a support of one voxel was used to partly suppress the noise in the volumes. A threshold was selected at 27% of the maximal gray scale value, which corresponds to the peak for bone tissue in the histogram of the gray value distribution in the image. In addition to bone volume, BMD was assessed.

In left unfractured legs BMD was analysed in a 1 mm thick region of interest in the distal femur metaphysis. BMD was analysed in the whole VOI (BMD_{all}), within trabecular bone in the VOI excluding cortical bone (BMD_{trab}) and within the inner 50% of the trabecular bone ($BMD_{trab50\%}$).

ELISA

After canulation of the right carotid artery and measurement of blood pressure at 2, 5 and 10 weeks, 1 mL blood was collected and serum was frozen at –80°C after centrifugation. Parathyroid hormone (PTH) was measured using a standard ELISA Kit (Mouse Intact PTH ELISA Kit, Immunotopics, San Clemente, Canada).

Statistical analysis

All data are given as means ± SEM. After proving normal distribution of the data and the assumption of equal variance, comparison between the experimental groups was performed by Student's *t*-test or one-way ANOVA and Student-Newman-Keuls *post hoc* test. For non-parametrical data, the Mann–Whitney test was used. Statistics were performed, using GraphPad Prism 4.0 (San Diego, CA, USA). A P-value < 0.05 was considered to indicate significant differences.

Results

Mean arterial blood pressure

Animals treated with the ACE inhibitor perindopril showed a significantly ($P < 0.05$) lower mean arterial pressure at 2, 5 and 10 (56.0 ± 5.8, 63.1 ± 6.3 and 66.3 ± 4.6 mmHg) weeks after fracture when compared with non-treated controls (84.0 ± 7.8, 91.3 ± 5.7 and 89.4 ± 5.8 mmHg).

Influence of perindopril treatment on unfractured bone
Micro-CT analysis revealed a significantly decreased BMD_{all} and BMD_{trab} in the distal femoral metaphysis after 10 weeks of perindopril treatment (Table 1).

Expression of ACE, AT_1 and AT_2 receptors during fracture healing
Immunohistological analysis of the callus 2 weeks after fracture showed expression of ACE during endochondral bone healing. ACE was found expressed in the periosteal callus at the zone of cartilage maturation by osteoblasts and hypertrophic chondrocytes (Figure 1A and B). We also observed expression of ACE during endochondral bone formation by osteoblasts in the growth plate of the proximal femur (Figure 1C). However, we did not observe expression of ACE in osteocytes in lamellar bone (Figure 1D). Western blot analysis confirmed expression of ACE in the healing callus after 2 weeks and further showed expression of AT_1 and AT_2 receptors (Figure 2). Quantitative analysis revealed that expression of ACE was significantly lower in the fracture callus of perindopril-treated animals compared with that of controls. In contrast, expression of AT_2 receptors was significantly greater in perindopril-treated animals, whereas no differences in expression of AT_1 receptors were observed (Figure 2).

Table 1 Micro-CT analysis of unfractured left femora after 10 weeks

Micro-CT analysis	*10 weeks*		
	Perindopril	*Control*	P
BMD_{all} (mgHA·mm^{-3})	327.0 ± 14.1	375.9 ± 16.26	<0.05
BMD_{trab} (mgHA·mm^{-3})	318.7 ± 14.3	368.1 ± 16.7	<0.05
$BMD_{trab50\%}$ (mgHA·mm^{-3})	60.14 ± 11.0	43.6 ± 13.7	0.36

Micro-CT analysis was performed in the distal metaphysis of unfractured left femora.
Data shown in the Table are mean ± SEM.
BMD, bone mineral density.

Radiological analysis
Two weeks after fracture there was a tendency towards a greater relative callus size in the perindopril-treated animals compared with controls. After 5 weeks the callus size showed no difference between the groups, whereas after 10 weeks the periosteal callus in the control animals was greater than in perindopril-treated animals (Table 2). Of interest, in control animals the relative callus size increased continuously from weeks 2 to 10, while in perindopril-treated animals, it had increased to maximum values by week 5 and it then significantly decreased until the end of the 10 week observation period (Table 2). The Goldberg score indicated an improved healing in perindopril-treated animals after 2 and 10 weeks. However, this difference did not prove to be statistically different (Table 2).

Histomorphometric analysis
Osteotomies healed predominantly by endochondral callus formation near the osteotomy gap and by intramembraneous

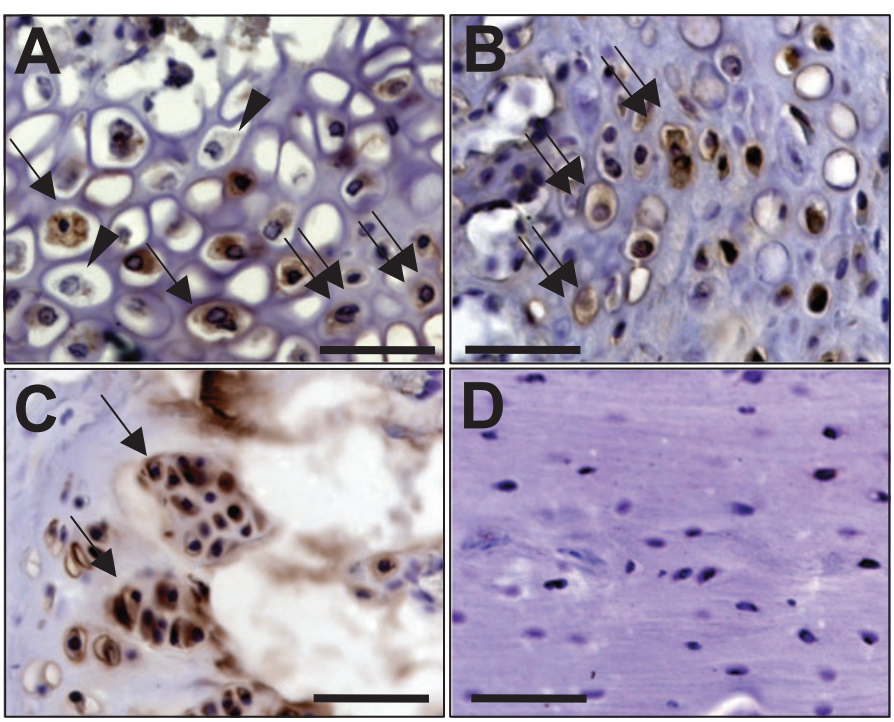

Figure 1 Immunohistochemical analysis of angiotensin-converting enzyme (ACE) expression in femora of untreated CD-1 mice 2 weeks after fracture and stabilization. (A) ACE expression in the periosteal callus at the zone of cartilage maturation by osteoblasts (double arrows) and hypertrophic chondrocytes (arrows). Of interest, not all of the chondrocytes stained positively for ACE (arrowheads). (B) ACE expression in the periosteal callus at the zone of cartilage maturation by osteoblasts (double arrows). (C) ACE expression in the growth plate of the proximal femur by osteoblasts (arrows) of a 9-week-old CD-1 mouse. (D) Lack of ACE expression in osteocytes of lamellar bone. Bar = 50 μm.

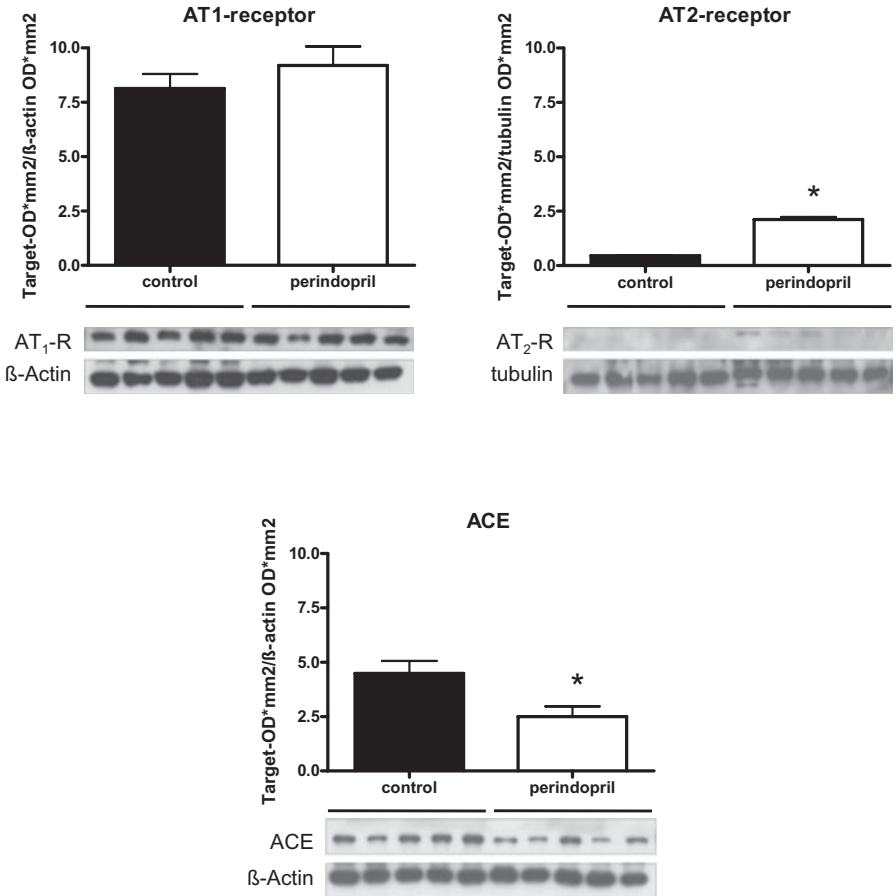

Figure 2 Western blot analysis of the expression of angiotensin-converting enzyme (ACE), AT_1 and AT_2 receptors in the periosteal callus after 2 weeks of fracture healing in perindopril-treated animals and untreated controls. Mean ± SEM (*$P < 0.05$ vs. control).

Table 2 Radiological, biomechanical and micro-CT analysis 2, 5 and 10 weeks after fracture of perindopril-treated and untreated animals

	2 weeks			*5 weeks*			*10 weeks*		
	Perindopril	*Control*	P	*Perindopril*	*Control*	P	*Perindopril*	*Control*	P
Radiology									
Cl.Dm/F.Dm (%)	111.3 ± 4.0	104.2 ± 2.1	0.14	139.7 ± 4[a]	134.1 ± 9.6	0.57	124.0 ± 5.1	137.3 ± 4.5	0.06
Goldberg score	0.5 ± 0.1	0.6 ± 0.2	0.14	1.3 ± 0.2	1.2 ± 0.2	0.80	1.6 ± 0.1	1.9 ± 0.1	0.08
Biomechanics									
Max. torque (%)	0.3 ± 0.0	0.1 ± 0.03	<0.001	97.2 ± 18.5	65.0 ± 12.6	0.18	80.3 ± 8.2	85.2 ± 6.6	0.65
Angle (%)	98.8 ± 16.5	81.3 ± 18.9	0.50	70.4 ± 6.5	94.9 ± 17.1	0.21	89.5 ± 18.8	82.4 ± 4.8	0.72
Stiffness (%)	0.5 ± 0.2	0.2 ± 0.1	0.12	148.1 ± 35.1	74.5 ± 13.0	0.07	113.6 ± 21.8	104.4 ± 6.9	0.70
Micro-CT analysis									
Bone volume (mm^3)							3.9 ± 0.2	4.7 ± 0.3	0.06
BMD ($mgHA{\cdot}mm^{-3}$)							1058.0 ± 7.6	1051.0 ± 10.5	0.60

Data are mean ± SEM.
[a]$P < 0.05$ versus perindopril-treated animals after 10 weeks.
BMD, bone mineral density; Cl.Dm/F.Dm, maximum callus diameter/femur diameter.

bone formation at some distance from the gap. At 2 and 5 weeks after fracture perindopril-treated animals showed a significantly greater periosteal callus formation compared with controls. This was indicated by a significantly greater relative callus diameter (Table 3). Accordingly, we observed also a significantly ($P < 0.05$) greater periosteal callus area after 2 and 5 weeks (Table 3). Additionally, animals treated with perindopril showed a higher healing score during this time period (Table 3). These differences were completely lost after 10 weeks. At this time point, all animals showed complete bone bridging of the osteotomy, resulting in a healing score of 4 (Table 3). Tissue composition of the periosteal callus did not differ significantly between the two groups studied. However, at 2 weeks after fracture perindopril-treated animals showed

Table 3 Histomorphometric analysis 2, 5 and 10 weeks after fracture of perindopril-treated and untreated animals

Histomorphometry	*2 weeks*			*5 weeks*			*10 weeks*		
	Perindopril	*Control*	P	*Perindopril*	*Control*	P	*Perindopril*	*Control*	P
Gap width (mm)	0.2 ± 0.0	0.2 ± 0.0[a]	0.29	0.0 ± 0.0	0.2 ± 0.1	<0.001	0.0 ± 0.0	0.0 ± 0.0	1.00
Cl.Dm/F.Dm (%)	211.3 ± 16.1	151.1 ± 17.3	0.02	164.1 ± 9.5	127.8 ± 8.6	<0.05	139.4 ± 6.0	137.7 ± 9.5	0.89
Pc.Ar (mm^2)	5.2 ± 0.6	2.1 ± 0.8	<0.01	3.2 ± 0.5	1.0 ± 0.4	<0.01	2.6 ± 0.4	2.5 ± 0.5	0.79
Bone/Pc.Ar (%)	42.9 ± 7.7	36.7 ± 10.4	0.64	96.4 ± 3.6	90.9 ± 9.1	0.53	100.0 ± 0.0	100.0 ± 0.0	1.00
Cartilage/ Pc.Ar (%)	40.5 ± 6.9	19.9 ± 9.4	0.10	0.3 ± 0.3	0.9 ± 0.9	0.42	0.0 ± 0.0	0.0 ± 0.0	1.00
F.t./Pc.Ar (%)	16.6 ± 1.7	43.4 ± 16.3	0.06	3.4 ± 3.4	8.3 ± 8.3	0.54	0.0 ± 0.0	0.0 ± 0.0	1.00
Healing score	1.3 ± 0.3	0.3 ± 0.2	<0.01	3.8 ± 0.7	2.0 ± 0.7	<0.05	4.0 ± 0.0	4.0 ± 0.0	1.00

Data shown in the Table are mean ± SEM.
[a]$P < 0.05$ versus perindopril-treated animals after 5 weeks.
Cl.Dm/F.Dm, maximum callus diameter/femur diameter; F.t., fibrous tissue; Pc.Ar, periosteal callus area.

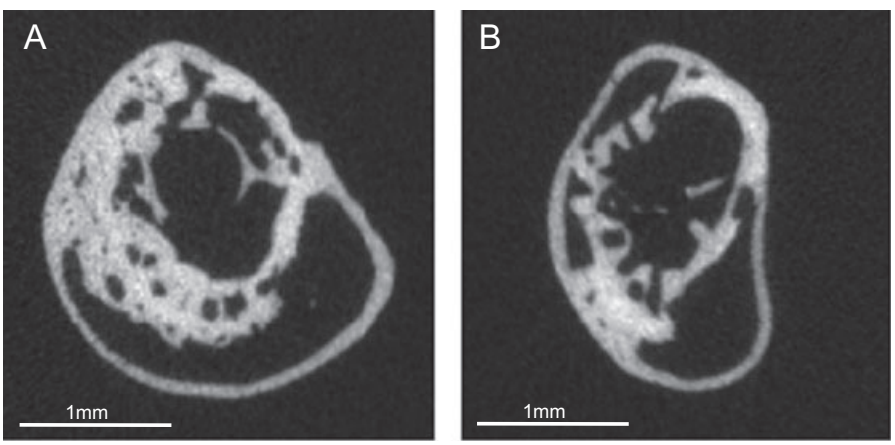

Figure 3 Representative micro-CT slices from the centre of the callus after 10 weeks of fracture healing in a control (A) and a perindopril-treated animal (B).

some more cartilage and markedly less fibrous tissue (Table 3). Of interest, we observed a significant ($P < 0.05$) reduction of the gap width from weeks 2 to 5 in the perindopril-treated animals, which was not observed in untreated controls. This resulted in a significantly smaller gap at week 5 after fracture in perindopril-treated animals (Table 3).

Biomechanical analysis
Biomechanical analysis at week 2 after fracture showed a significantly ($P < 0.05$) greater maximal torque at failure and a higher torsional stiffness in perindopril-treated animals compared with controls (Table 2). After 5 weeks, maximal torque and torsional stiffness were still greater after perindopril treatment; however, these differences did not prove statistically significant (Table 2). After 10 weeks, both groups showed complete bone healing, as indicated by a torsional stiffness of almost 100% of the contralateral femur in both groups (Table 2).

Micro-CT analysis
After 10 weeks, BMD in the gap region was not different between the two groups. However, according to the X-ray analysis, bone volume was smaller in perindopril-treated animals compared with controls (Table 2 and Figure 3).

Proliferation and apoptosis in the periosteal callus
Expression of PCNA, as an indicator of cell proliferation in the fracture callus, showed no difference between both groups. Expression of cleaved caspase-3 in the fracture callus indicated a significantly decreased apoptosis in the perindopril-treated group compared with controls (Figure 4).

PTH-serum concentration
ELISA analysis of PTH serum concentrations showed no difference between perindopril-treated animals and controls. We also could not detect any significant differences over the time course of fracture healing (data not shown).

Discussion

In the present study, we showed for the first time, expression of components of the RAS during fracture healing *in vivo*. Osteoblasts and hypertrophic chondrocytes expressed ACE

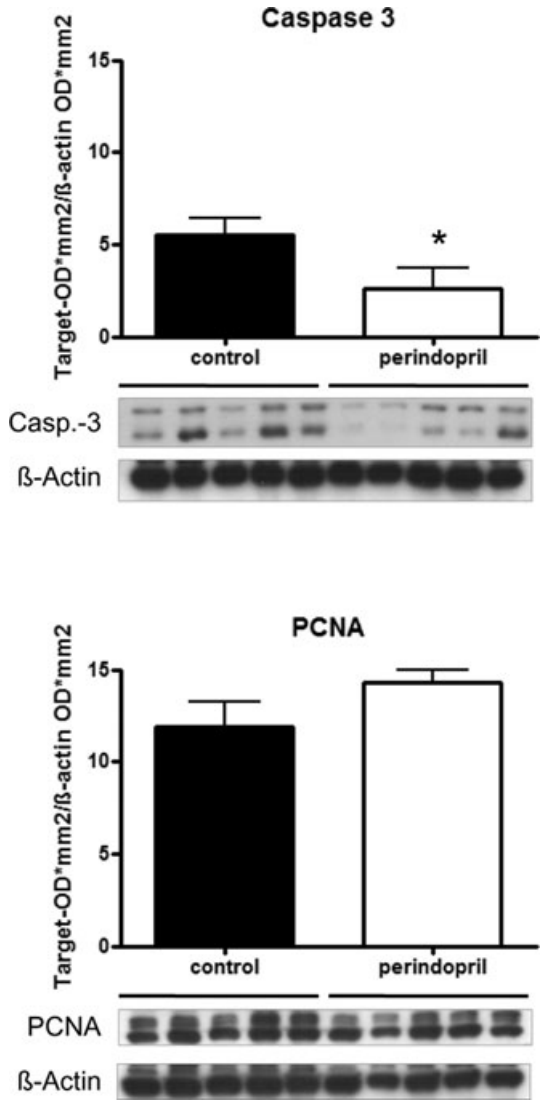

Figure 4 Western blot analysis of cleaved caspase-3 and proliferating cell nuclear antigen (PCNA) expression in the periosteal callus after 2 weeks of fracture healing in perindopril-treated animals and untreated controls. Mean ± SEM (*$P < 0.05$ vs. control).

during endochondral bone formation in the periosteal callus area. Expression was localized in the zone of cartilage maturation and hypertrophy. Recently Izu *et al.* (2009) showed expression of RAS components during normal bone growth. They showed expression of ACE in osteoblasts during endochondral bone formation in the growth plate. However, in contrast to our findings they did not report expression of ACE by chondrocytes in the growth plate. This might be due to different phenotypes of chondrocytes during endochondral bone formation in the growth plate compared with fracture healing. Furthermore, chondrocytes do not consistently undergo the same process of terminal differentiation and maturation during endochondral bone formation. Indeed, not all chondrocytes in the periosteal callus showed expression of ACE during endochondral fracture healing (Figure 1A).

Inhibition of ACE with perindopril resulted in a reduced expression of ACE in the healing callus, as indicated by Western blot analysis after 2 weeks of fracture healing. The down-regulation of ACE after ACE inhibition is in line with the results of studies in other tissues with a local RAS (Zhuo *et al.*, 2002; Hamming *et al.*, 2008). Interestingly, we observed a higher expression of AT_2 receptors after ACE inhibition, however, no difference in AT_1 receptor expression. Whereas different studies have shown that Ang II down-regulates its own receptors (Iwai *et al.*, 1991; Iwai and Inagami, 1992), there are conflicting reports about the regulation of the AT_1 and AT_2 receptors after ACE inhibition (Ouali *et al.*, 1997; Zhu *et al.*, 1999; Xu *et al.*, 2002).

Angiotensin-converting enzyme inhibition during fracture healing resulted in an increased periosteal callus formation after 2 and 5 weeks. This was most probably due to a decrease of apoptotic cell death in the periosteal callus and not due to an increase of cell proliferation, as indicated by an unchanged PCNA but a decreased cleaved caspase-3 expression. The improved periosteal callus formation resulted in an accelerated healing process with an earlier histological bridging of the fracture gap and an advanced remodelling after 10 weeks.

The improved histological healing of the fractures after perindopril treatment is further supported by the results of our biomechanical analysis, which demonstrated a greater torque to failure and a higher torsional stiffness after 2 and 5 weeks in perindopril-treated animals. Of interest, after 2 weeks of fracture healing, the periosteal callus of perindopril-treated animals showed less fibrous tissue compared with controls. Different studies have shown that the RAS contributes to fibrogenesis in a variety of organs like the heart, vascular wall, pancreas, kidney and liver (Kuno *et al.*, 2003; Sun and Weber, 2003; Ikura *et al.*, 2005; Morihara *et al.*, 2006; Shirazi *et al.*, 2007). Accordingly, the reduced fibrous tissue in the periosteal callus area of perindopril-treated animals is compatible with the results of other studies, which have shown reduced fibrous tissue formation after blockade of the RAS (Yoshiji *et al.*, 2007).

The ACE is a key component of the RAS, generating Ang II as the main effector molecule. Different *in vitro* studies have shown that Ang II can be synthesized by osteoblastic cells through ACE and that Ang II influences osteoblastic cell functions through specific receptor binding (Hatton *et al.*, 1997; Hiruma *et al.*, 1997; Hagiwara *et al.*, 1998; Schurman *et al.*, 2004). Ang II exerts its biological effects mainly by two receptors, the AT_1 and AT_2 receptors. Ang II has a multitude of biological effects in different tissues and influences inflammation, angiogenesis, cell proliferation, cell differentiation and apoptosis (Haulica *et al.*, 2005). Accordingly, the RAS has been shown to significantly influence tissue remodelling in various tissues (Haulica *et al.*, 2005). We demonstrate now for the first time the expression of ACE, AT_1 and AT_2 receptors during fracture healing *in vivo*. Both receptors are known to induce apoptosis in different cell types (Dimmeler *et al.*, 1997; Bonnet *et al.*, 2001; Haulica *et al.*, 2005). Vice versa, ACE inhibition has been shown to decrease apoptosis in various tissues (Diez *et al.*, 1997; Odaka and Mizuochi, 2000; Matsumoto *et al.*, 2003).

Because perindopril treatment significantly lowered the MAP, it remains possible that the improvement of fracture healing was due to the perindopril-associated reduction of blood pressure, rather than a direct pharmacological action of

perindopril. Herein, we have shown that perindopril significantly lowered the BMD in unfractured femora compared with controls. These data may help to decide whether the reduced MAP after perindopril treatment may have contributed to the improved fracture healing. MAP influences bone metabolism, because it determines intramedullar pressure that is a driving force for transcortical interstitial fluid (ISF) flow. Whereas intramedullar pressure remains essentially constant above a MAP of 81 mmHg, it decreases when MAP is lowered under 81 mmHg, thereby reducing ISF flow (Tondevold *et al.*, 1979). The current hypothesis suggests that ISF flow mediates the effects of physical strain on bone. This hypothesis is supported by space-flight and tail suspendent rat models, which showed that ISF flow is an integral mechanism of skeletal adoption (McCarthy, 2005). An increased intramedullar pressure has been shown to increase BMD due to an increased ISF flow (Hillsley and Frangos, 1994). Vice versa, in microgravity or in bedrest studies a decreased BMD of the lower extremities has been associated with a decreased intramedlluar pressure due to cephalic fluid shift with subsequent reduction in capillary pressure (Hillsley and Frangos, 1994). Thus, the decreased BMD observed in unfractured femora in the present study is most probably due to the decreased MAP.

There is no information on whether a reduced intramedullar pressure and a reduced ISF flow influences fracture healing. However, Pearse and Morton demonstrated as early as 1930 that a venous tourniquet stimulates bone growth in patients with delayed fracture healing (Pearse and Morton, 1930). Later studies have shown that a venous tourniquet or intermittent pneumatic compression increase intramedullar pressure as well as ISF flow (Kelly and Bronk, 1990) and have confirmed consequent stimulation of fracture healing (Kruse and Kelly, 1974; Hewitt *et al.*, 2005). The molecular basis of these findings might be an up-regulation of NO and PGs due to the increased ISF flow (Johnson *et al.*, 1996; Mcallister *et al.*, 2000; Bakker *et al.*, 2001), both of which are known to stimulate fracture healing (Diwan *et al.*, 2000; Xie *et al.*, 2009).

Because a decrease of MAP results in a reduced intramedullar pressure and a reduced ISF flow, a decreased callus formation and an impaired healing with reduced bone formation would be expected. However, in the present study we did not observe decreased bone or callus formation after perindopril treatment despite the significant reduction of MAP. We also did not find a decreased BMD in the remodelling phase of fracture healing at 10 weeks. In contrast, we observed a stimulation of fracture healing with an increased periosteal callus formation and an improved biomechanical stiffness in perindopril-treated animals. Thus, we conclude that the improved fracture healing by perindopril is more probably due to a direct pharmacological action rather than due to the perindopril-associated reduction in blood pressure.

One link between blood pressure, antihypertensive drugs and bone metabolism might be a disturbed calcium metabolism, which is affected after ACE inhibition and subsequently influences systemic PTH levels (Nakagami *et al.*, 2007). Because PTH has recently been recognized to improve fracture healing by increasing callus formation and accelerating the healing process, we also studied systemic PTH levels (Nakajima *et al.*, 2002; Barnes *et al.*, 2008). However, we could not detect any significant difference in PTH levels at any time during perindopril treatment. Thus, the improvement of fracture healing by ACE inhibition, observed in the present study, was independent of any actions on PTH.

Because ACE inhibitors are widely used in cardiovascular medicine, it is of particular interest to elucidate how these drugs may interfere with bone homeostasis. While the present study shows that hypotension induced by ACE inhibition reduced BMD, clinical studies have provided evidence that, under normotensive and hypertensive conditions, ACE inhibition actually increased BMD, in particular in the elderly (Lynn *et al.*, 2006). Consistent with this, normotensive patients with an I/I polymorphism and low ACE activity also show an increased BMD (Perez-castrillon *et al.*, 2003a). Our present data may encourage a clinical study to analyse whether fracture healing is also improved in patients with cardiovascular disorders treated with ACE inhibitors.

Acknowledgements

We thank Janine Becker for excellent technical assistance. This study was supported by a grant of the AO foundation, Switzerland.

Conflicts of interest

None.

References

Alexander SPH, Mathie A, Peters JA (2009). Guide to Receptors and Channels (GRAC), 4th edn. *Br J Pharmacol* **158** (Suppl. 1): S1–S254.

Bakker AD, Soejima K, Klein-Nulend J, Burger EH (2001). The production of nitric oxide and prostaglandin E(2) by primary bone cells is shear stress dependent. *J Biomech* **34**: 671–677.

Barnes GL, Kakar S, Vora S, Morgan EF, Gerstenfeld LC, Einhorn TA (2008). Stimulation of fracture-healing with systemic intermittent parathyroid hormone treatment. *J Bone Joint Surg Am* **90** (Suppl. 1): 120–127.

Bonnet F, Cao Z, Cooper ME (2001). Apoptosis and angiotensin II: yet another renal regulatory system? *Exp Nephrol* **9**: 295–300.

Diez J, Panizo A, Hernandez M, Vega F, Sola I, Fortuno MA *et al.* (1997). Cardiomyocyte apoptosis and cardiac angiotensin-converting enzyme in spontaneously hypertensive rats. *Hypertension* **30**: 1029–1034.

Dimmeler S, Rippmann V, Weiland U, Haendeler J, Zeiher AM (1997). Angiotensin II induces apoptosis of human endothelial cells. Protective effect of nitric oxide. *Circ Res* **81**: 970–976.

Diwan AD, Wang MX, Jang D, Zhu W, Murrell GA (2000). Nitric oxide modulates fracture healing. *J Bone Miner Res* **15**: 342–351.

Garcia P, Holstein JH, Histing T, Burkhardt M, Culemann U, Pizanis A *et al.* (2008a). A new technique for internal fixation of femoral fractures in mice: impact of stability on fracture healing. *J Biomech* **41**: 1689–1696.

Garcia P, Holstein JH, Maier S, Schaumloffel H, Al-Marrawi F, Hannig M *et al.* (2008b). Development of a reliable non-union model in mice. *J Surg Res* **147**: 84–91.

Goldberg VM, Powell A, Shaffer JW, Zika J, Bos GD, Heiple KG (1985). Bone grafting: role of histocompatibility in transplantation. *J Orthop Res* **3**: 389–404.

Hagiwara H, Hiruma Y, Inoue A, Yamaguchi A, Hirose S (1998). Deceleration by angiotensin II of the differentiation and bone formation of rat calvarial osteoblastic cells. *J Endocrinol* **156**: 543–550.

Hamming I, van Goor H, Turner A, Rushworth C, Michaud A, Corvol P *et al*. (2008). Differential regulation of renal ACE2 and ACE during ACE inhibition and dietary sodium restriction in healthy rats. *Exp Physiol* **93**: 631–638.

Hatton R, Stimpel M, Chambers TJ (1997). Angiotensin II is generated from angiotensin I by bone cells and stimulates osteoclastic bone resorption *in vitro*. *J Endocrinol* **152**: 5–10.

Haulica I, Bild W, Serban DN (2005). Angiotensin peptides and their pleiotropic actions. *J Renin Angiotensin Aldosterone Syst* **6**: 121–131.

Hewitt JD, Harrelson JM, Dailiana Z, Guilak F, Fink C (2005). The effect of intermittent pneumatic compression on fracture healing. *J Orthop Trauma* **19**: 371–376.

Hillsley MV, Frangos JA (1994). Bone tissue engineering: the role of interstitial fluid flow. *Biotechnol Bioeng* **43**: 573–581.

Hiruma Y, Inoue A, Hirose S, Hagiwara H (1997). Angiotensin II stimulates the proliferation of osteoblast-rich populations of cells from rat calvariae. *Biochem Biophys Res Commun* **230**: 176–178.

Holstein JH, Menger MD, Culemann U, Meier C, Pohlemann T (2007). Development of a locking femur nail for mice. *J Biomech* **40**: 215–219.

Ikura Y, Ohsawa M, Shirai N, Sugama Y, Fukushima H, Suekane T *et al*. (2005). Expression of angiotensin II type 1 receptor in human cirrhotic livers: Its relation to fibrosis and portal hypertension. *Hepatol Res* **32**: 107–116.

Iwai N, Inagami T (1992). Regulation of the expression of the rat angiotensin II receptor mRNA. *Biochem Biophys Res Commun* **182**: 1094–1099.

Iwai N, Yamano Y, Chaki S, Konishi F, Bardhan S, Tibbetts C *et al*. (1991). Rat angiotensin II receptor: cDNA sequence and regulation of the gene expression. *Biochem Biophys Res Commun* **177**: 299–304.

Izu Y, Mizoguchi F, Kawamata A, Hayata T, Nakamoto T, Nakashima K *et al*. (2009). Angiotensin II type 2 receptor blockade increases bone mass. *J Biol Chem* **284**: 4857–4864.

Johnson DL, McAllister TN, Frangos JA (1996). Fluid flow stimulates rapid and continuous release of nitric oxide in osteoblasts. *Am J Physiol* **271**: E205–E208.

Kelly PJ, Bronk JT (1990). Venous pressure and bone formation. *Microvasc Res* **39**: 364–375.

Kruse RL, Kelly PJ (1974). Acceleration of fracture healing distal to a venous tourniquet. *J Bone Joint Surg Am* **56**: 730–739.

Kuno A, Yamada T, Masuda K, Ogawa K, Sogawa M, Nakamura S *et al*. (2003). Angiotensin-converting enzyme inhibitor attenuates pancreatic inflammation and fibrosis in male Wistar Bonn/Kobori rats. *Gastroenterology* **124**: 1010–1019.

Lynn H, Kwok T, Wong SY, Woo J, Leung PC (2006). Angiotensin converting enzyme inhibitor use is associated with higher bone mineral density in elderly Chinese. *Bone* **38**: 584–588.

McAllister TN, Du T, Frangos JA (2000). Fluid shear stress stimulates prostaglandin and nitric oxide release in bone marrow-derived preosteoclast-like cells. *Biochem Biophys Res Commun* **270**: 643–648.

McCarthy ID (2005). Fluid shifts due to microgravity and their effects on bone: a review of current knowledge. *Ann Biomed Eng* **33**: 95–103.

Matsumoto N, Manabe H, Ochiai J, Fujita N, Takagi T, Uemura M *et al*. (2003). An AT1-receptor antagonist and an angiotensin-converting enzyme inhibitor protect against hypoxia-induced apoptosis in human aortic endothelial cells through upregulation of endothelial cell nitric oxide synthase activity. *Shock* **19**: 547–552.

Morihara K, Takai S, Takenaka H, Sakaguchi M, Okamoto Y, Morihara T *et al*. (2006). Cutaneous tissue angiotensin-converting enzyme may participate in pathologic scar formation in human skin. *J Am Acad Dermatol* **54**: 251–257.

Nakagami H, Osako MK, Shimizu H, Hanayama R, Morishita R (2007). Potential contribution of action of renin angiotensin system to bone metabolism. *Curr Hypertens Rev* **3**: 129–132.

Nakajima A, Shimoji N, Shiomi K, Shimizu S, Moriya H, Einhorn TA *et al*. (2002). Mechanisms for the enhancement of fracture healing in rats treated with intermittent low-dose human parathyroid hormone (1–34). *J Bone Miner Res* **17**: 2038–2047.

Odaka C, Mizuochi T (2000). Angiotensin-converting enzyme inhibitor captopril prevents activation-induced apoptosis by interfering with T cell activation signals. *Clin Exp Immunol* **121**: 515–522.

Ouali R, Berthelon MC, Begeot M, Saez JM (1997). Angiotensin II receptor subtypes AT1 and AT2 are down-regulated by angiotensin II through AT1 receptor by different mechanisms. *Endocrinology* **138**: 725–733.

Paul M, Poyan Mehr A, Kreutz R (2006). Physiology of local renin-angiotensin systems. *Physiol Rev* **86**: 747–803.

Pearse HEJ, Morton JJ (1930). The stimulation of bone gowth by venous stasis. *J Bone Joint Surg Am* **12**: 97–111.

Perez-Castrillon JL, Justo I, Silva J, Sanz A, Martin-Escudero JC, Igea R *et al*. (2003a). Relationship between bone mineral density and angiotensin converting enzyme polymorphism in hypertensive postmenopausal women. *Am J Hypertens* **16**: 233–235.

Perez-Castrillon JL, Silva J, Justo I, Sanz A, Martin-Luquero M, Igea R *et al*. (2003b). Effect of quinapril, quinapril-hydrochlorothiazide, and enalapril on the bone mass of hypertensive subjects: relationship with angiotensin converting enzyme polymorphisms. *Am J Hypertens* **16**: 453–459.

Rejnmark L, Vestergaard P, Mosekilde L (2006). Treatment with beta-blockers, ACE inhibitors, and calcium-channel blockers is associated with a reduced fracture risk: a nationwide case-control study. *J Hypertens* **24**: 581–589.

Schurman SJ, Bergstrom WH, Shoemaker LR, Welch TR (2004). Angiotensin II reduces calcium uptake into bone. *Pediatr Nephrol* **19**: 33–35.

Sernia C, Huang H, Nguyuen K, Li Y-H, Hsu S, Chen M *et al*. (2008). *Bone Homeostasis: An Emerging Role for the Renin-Angiotensin System*. Springer: Dordrecht, The Netherlands.

Shirazi M, Noorafshan A, Bahri MA, Tanideh N (2007). Captopril reduces interstitial renal fibrosis and preserves more normal renal tubules in neonatal dogs with partial urethral obstruction: a preliminary study. *Urol Int* **78**: 173–177.

Sun Y, Weber KT (2003). RAS and connective tissue in the heart. *Int J Biochem Cell Biol* **35**: 919–931.

Tondevold E, Eriksen J, Jansen E (1979). Observations on long bone medullary pressure in relation to mean arterial blood pressure in the anaesthetized dog. *Acta Orthop Scand* **50**: 527–531.

Woods D, Onambele G, Woledge R, Skelton D, Bruce S, Humphries SE *et al*. (2001). Angiotensin-I converting enzyme genotype-dependent benefit from hormone replacement therapy in isometric muscle strength and bone mineral density. *J Clin Endocrinol Metab* **86**: 2200–2204.

Xie C, Liang B, Xue M, Lin AS, Loiselle A, Schwarz EM *et al*. (2009). Rescue of impaired fracture healing in COX-2-/- mice via activation of prostaglandin E2 receptor subtype 4. *Am J Pathol* **175**: 772–785.

Xu Y, Kumar D, Dyck JR, Ford WR, Clanachan AS, Lopaschuk GD *et al*. (2002). AT(1) and AT(2) receptor expression and blockade after acute ischemia-reperfusion in isolated working rat hearts. *Am J Physiol Heart Circ Physiol* **282**: H1206–H1215.

Yoshiji H, Kuriyama S, Fukui H (2007). Blockade of renin-angiotensin system in antifibrotic therapy. *J Gastroenterol Hepatol* **22** (Suppl. 1): S93–S95.

Zhu YC, Zhu YZ, Li J, Schafer H, Schmidt WE, Unger T *et al*. (1999). Effects of ramipril on cardiac gene transcription levels of angiotensin II receptors after myocardial infarction. *Zhongguo Yao Li Xue Bao* **20**: 481–485.

Zhuo JL, Mendelsohn FA, Ohishi M (2002). Perindopril alters vascular angiotensin-converting enzyme, AT(1) receptor, and nitric oxide synthase expression in patients with coronary heart disease. *Hypertension* **39**: 634–638.